Resist-Dyed Textile Alkaline Zn Microbatteries with Significantly Suppressed Zn Dendrite Growth

Mengmeng Liu,[†,‡] Xiong Pu,*[,†,‡,§] Zifeng Cong,[†,‡] Zhixiao Liu,[‖] Ting Liu,[†,‡] Yanghui Chen,[†,‡] Jianqiang Fu,[†,‡] Weiguo Hu,*[,†,‡,§] and Zhong Lin Wang*[,†,‡,§,⊥]

[†]CAS Center for Excellence in Nanoscience, Beijing Key Laboratory of Micro-Nano Energy and Sensor, Beijing Institute of Nanoenergy and Nanosystems, Chinese Academy of Sciences, Beijing 100083, China

[‡]School of Nanoscience and Technology, University of Chinese Academy of Sciences, Beijing 100049, China

[§]Center on Nanoenergy Research, School of Physical Science and Technology, Guangxi University, Nanning 530004, China
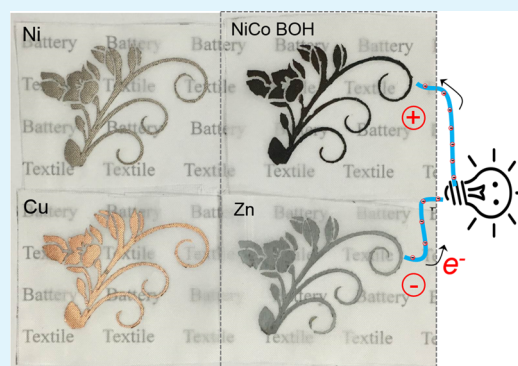
[‖]College of Materials Science and Engineering, Hunan University, Changsha 410082, China

[⊥]School of Materials Science and Engineering, Georgia Institute of Technology, Atlanta, Georgia 30332-0245, United States

Ⓢ *Supporting Information*

ABSTRACT: The progress of electronic textiles relies on the development of sustainable power sources without much sacrifice of convenience and comfort of fabrics. Herein, we present a rechargeable textile alkaline Zn microbattery (micro-AZB) fabricated by a process analogous to traditional resist-dyeing techniques. Conductive patterned electrodes are realized first by resist-aided electroless/electrodeposition of Ni/Cu films. The resulting coplanar micro-AZB in a single textile, with an electroplated Zn anode and a $Ni_{0.7}Co_{0.3}OOH$ cathode, achieves high energy density (256.2 Wh kg^{-1}), high power density (10.3 kW kg^{-1}), and stable cycling performances (82.7% for 1500 cycles). The solid-state micro-AZB also shows excellent mechanical reliability (bending, twisting, tailoring, etc.). The improved reversibility and cyclability of textile Zn electrodes over conventional Zn foils are found to be due to the significantly inhibited Zn dendrite growth and suppressed undesirable side reactions. This work provides a new approach for energy-storage textile with high rechargeability, high safety, and aesthetic design versatility.

KEYWORDS: *resist dyeing, Zn battery, electronic textile, wearable*

INTRODUCTION

Electronic textiles are emerging as ideal platforms of wearable electronics with various electronic components (transistors,[1,2] light-emitting diodes (LEDs),[3] displays,[4] and sensors[5−8]) integrated in fibers/yarns/fabrics for applications such as sports/healthcare monitoring, personal thermal management, and even medical therapy. One of the essential challenges is to power these textile electronics without much sacrifice of convenience, softness, and comfort of fabrics. Therefore, efforts have been recently devoted worldwide to developing wearable textile-based energy-storage devices such as supercapacitors (SCs) and lithium-ion batteries (LIBs). Though SCs feature high power density and safety, the insufficient energy density limits their applications; nonaqueous LIBs possess significantly higher energy density but suffer from intrinsic safety and cost issues.[9] Rechargeable aqueous zinc batteries are expected to be more promising as textile power sources owing to their combined advantages of high energy density, safety, and low cost.[10−14]

Metallic zinc is an ideal anode for aqueous batteries due to its two-electron redox reaction, low redox potential, and high abundance. A large family of Zn batteries has been studied, such as Zn−NiOOH,[10] Zn−Ag$_2$O,[15] Zn−air,[16−19] and Zn−MnO$_2$[20] batteries. Nevertheless, one long-lasting challenge for rechargeable Zn batteries is their unsatisfactory cycling stability originating mainly from the Zn dendritic growth. Recently, progresses have been made to suppress the dendrite formation by modifying the electrolyte with concentrated additives[21] or designing three-dimensional (3D) porous Zn as the anode, such as hierarchical ZnO/Zn on carbon cloth,[22,23] Zn nanosheets on carbon nanotube (CNT) paper,[24] and 3D Zn sponges.[10] Yet, very few works have been reported to realize flexible/wearable Zn batteries, and the research on suppressing Zn dendrite growth is still insufficient.

The mostly investigated approach for wearable textile energy devices is to fabricate one-dimensional fiber/yarn-shaped supercapacitors/batteries, which can be later woven into fabrics. Fiber/yarn-shaped supercapacitors,[25−28] lithium-ion batteries,[29−31] sodium-ion batteries,[32] and recently zinc batteries have been reported. Another alternative approach is
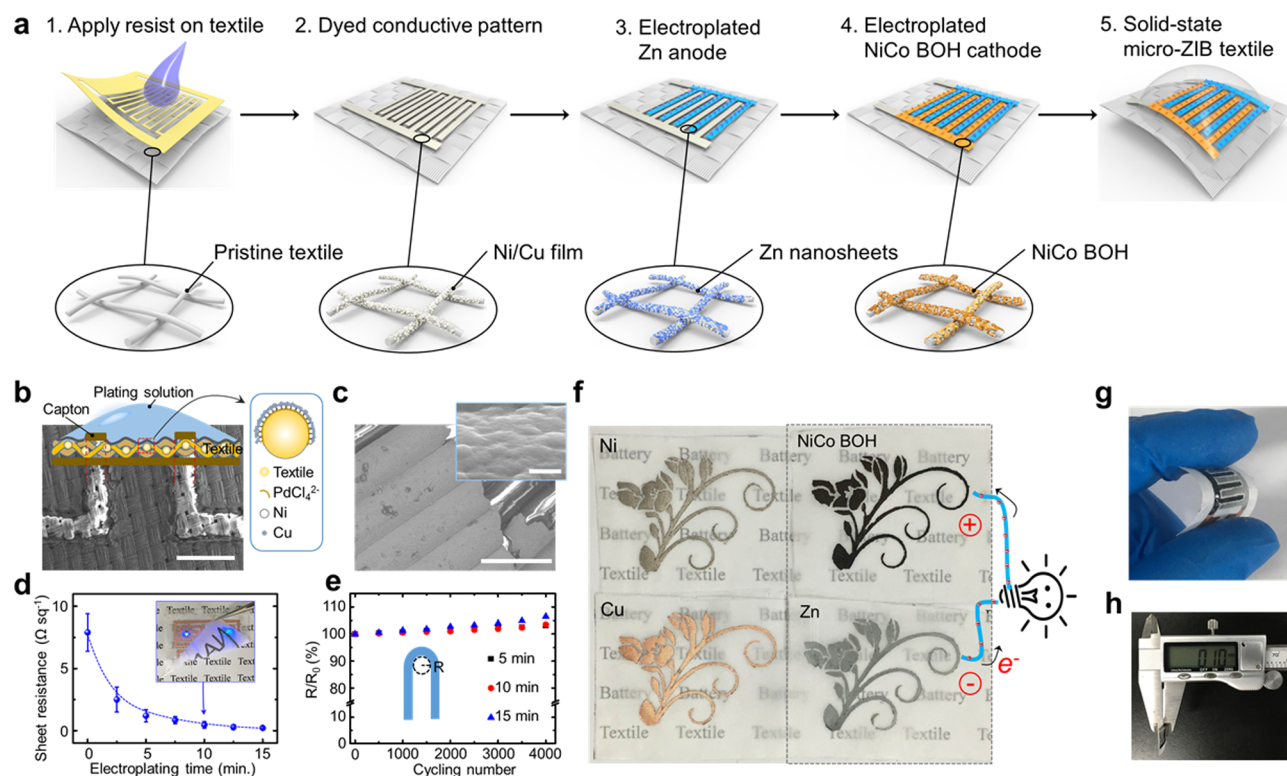
Figure 1. Fabrication of textile electrodes and micro-AZBs. (a) Schematic illustration of the fabrication procedures of textile micro-AZB. (b) Scanning electron microscopy (SEM) image of a Cu-coated finger electrode on the textile. (c) SEM images of Cu films. (d) Electrical properties and (e) bending stability of the Cu textile. The inset of (d) shows blue LEDs lighted through a Cu textile circuit under bending condition. (f) Photo of flowers fabricated on polyester fabrics with different coatings (Ni, Cu, Zn, NiCo BOH). (g) Photo shows a bended textile micro-AZB. (h) Thickness of a micro-AZB (0.1 mm). Scale bars, 1 mm (b), 30 μm (c), and 500 nm the inset of (c).

to directly load electrode materials on two-dimensional fabrics through dip-coating or printing methods and then assemble textile electrodes into a stacked sandwich architecture. Compared with these two approaches, in-plane microbatteries are more favorable for textile energy devices considering their higher electrochemical performances and better versatility in stylish designs.[33] However, common fabrication techniques based on photolithography and metal sputtering coating are inapplicable to textile substrate with wavy porous surfaces. Resist dyeing has been a widespread method for applying predesigned color patterns on fabrics since ancient times. Certain areas of fabrics are free to absorb the dye, whereas the undesired areas are blocked by the resist substance such as wax, rice paste, stencils, and string (tie dyeing). After the dyeing process and removal of the resist, aesthetic patterns with fascinating colors are obtained. By replacing the dye with conductive or electrode materials, it is possible to fabricate in-plane microbatteries with arbitrary designs.

In this work, we developed a novel resist-dyeing process to fabricate patterned conductive metal films and in-plane alkaline Zn microbatteries (micro-AZBs) on textile substrate. Laser-scribed Kapton film attached on the textile functions as the resist, and electroless deposition of Ni is analogous to the dyeing process. Once the conductive pattern of Ni film is deposited, various different materials can be electrodeposited above it, such as Cu, Zn, and Ni−Co bimetallic oxyhydroxide (NiCo BOH). Compared with the previously reported dip-coating, painting, or inkjet/screen printing of conductive carbonaceous materials, the thin Cu film offers significantly improved electron transfer (sheet resistance 0.22 Ω sq^{-1}) and

simultaneously maintains the light weight and softness of pristine textiles. Therefore, the textile micro-AZBs, with Zn as the anode and $(Ni_{0.7}Co_{0.3})OOH$ as the cathode, achieved both high energy density (256.2 Wh kg^{-1}) and high power density (10.3 kW kg^{-1}). By applying the gel-type electrolyte, solid-state micro-AZBs fabricated on common cloth also showed excellent mechanical reliability (bending, twisting, cutting, etc.). Impressively, the textile Zn anode exhibited improved cycling stability and reversibility and significantly suppressed dendrite growth compared with the Zn foil electrode mainly due to porous nature of fabrics and uniform nanosheet morphology of the electroplated Zn.

■ RESULTS AND DISCUSSION

Resist dyeing was adopted for the fabrication of patterned textiles and micro-AZBs, as illustrated in Figure 1a. A pristine polyester textile was sealed by a Kapton resist with desired patterns, which undergoes the electroless deposition of Ni coating and subsequent electrodeposition of Cu coating. During the processes of electroless- and electrodeposition, the Kapton mask functions as a resist to prevent ions ($PdCl_4^{2-}$, Ni^{2+}, Cu^{2+}, etc.) in aqueous solution from reaching the surfaces of sealed textile fibers. This process is analogous to the traditional tie dyeing, where the exposed area is dyed but not the pinched or sealed area (Figure S1). After removing the Kapton mask, two Cu electrodes with interdigitated configuration were coated on the textile substrate. Then, Zn and NiCo BOH nanosheets were electrodeposited on each of the Cu electrode, followed by applying aqueous or gel-type
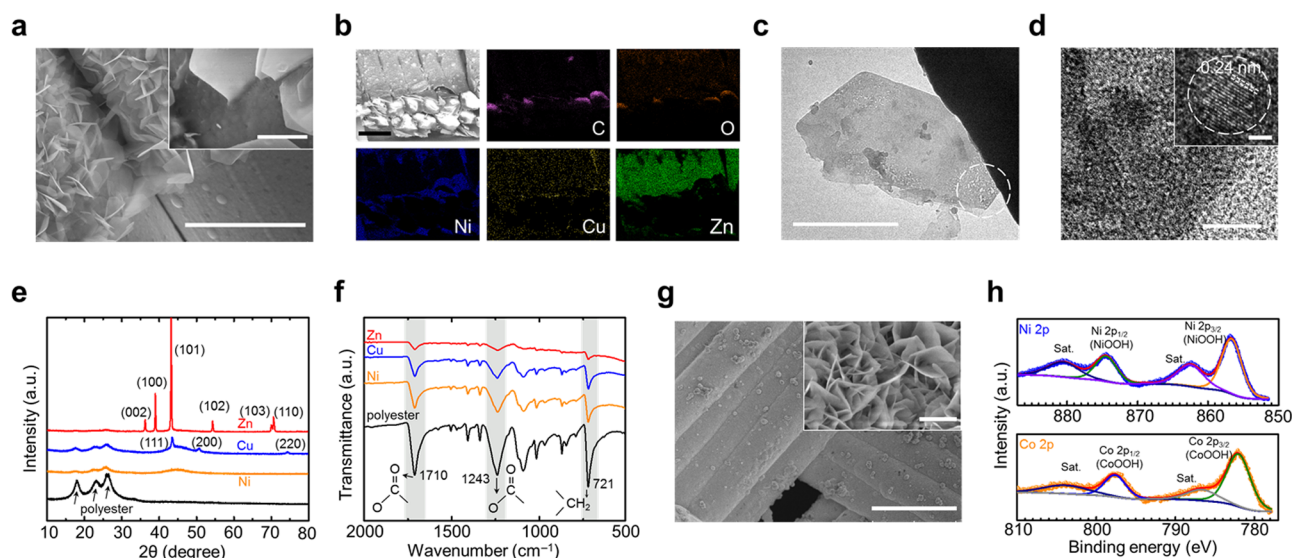
Figure 2. Morphology and structure characterization of the Zn and NiCo BOH electrodes. (a) SEM images of the Zn nanosheets on the Cu textile substrate. (b) SEM images and energy-dispersive X-ray spectroscopy (EDS) elemental mapping of the cross-section surface of a Zn electrode. (c, d) TEM images of the Zn nanosheets. (e) X-ray diffraction (XRD) profile and (f) Fourier transform infrared (FTIR) spectra of the pristine textile, Ni-coated textile, Cu-coated textile, and Zn-coated textile. (g) SEM images and (h) X-ray photoelectron spectrum (XPS) of Ni 2p and Co 2p of NiCo BOH. Scale bars, 5 μm (a), 1 μm (the inset of (a)), 30 μm (b), 500 nm (c), 10 nm (d), 2 nm (the inset of (d)), 50 μm (g), and 500 nm (the inset of (g)).

electrolyte to prepare aqueous or solid-state textile micro-AZBs, respectively.

Detailed schematic illustration is shown in Figure S2. The Ni coating was only deposited on the sensitized area, where the fiber surfaces were exposed to PdCl$_4^{2-}$ adsorption, whereas the subsequent electrodeposited coatings (Cu, Zn, NiCo BOH) can only be formed on top of conductive Ni films, leaving the sealed area as an insulating gap. The final gap size is close to that of the pristine Kapton resist (Figure 1b). The smallest gap size was achieved to be 0.3 mm. The woven textured feature of pristine fabrics was always maintained (see Figures 1b and S3a for optical microscope images). The conformal films of Ni and Cu nanoparticles wrapping up polyester fibers can be clearly observed from SEM images (Figures 1c and S4). The electrodeposited Cu film is smoother and has a smaller contact angle than the Ni film, favoring the uniform electrodeposition of Zn and NiCo BOH nanosheets (Figure S5).

Moreover, the Cu textile possesses simultaneously high electrical conductivity and flexibility. The sheet resistances of the Cu textile were about 1.1, 0.3, and 0.22 Ω sq^{-1} when the deposition times were 5, 10, and 15 min, respectively (see Figure 1d). The estimated electrical conductivity (σ) for the 15 min electrodeposition sample was about 1.13 × 10^4 S cm^{-1}. This value is much higher than most reported conductive films, such as silver elastomeric fibers,[34] layer-by-layer Au/Mxene on paper,[35,36] screen-printing carbon nanotube (CNT) silks,[37,38] screen-printing Zn textiles,[15] and dip-coating CNT fabrics[39] (Figure S6a). The Cu textiles were bent repeatedly to evaluate mechanical properties. After 4000 bending cycles at 2.7 mm of curvature radius, the sheet resistance increased slightly by 6.5, 3.4, and 3.1% for Cu textiles with 15, 10, and 5 min deposition times, respectively (see Figure 1e). Moreover, the Zn electrodes prepared by the screen-printing method and our resist-dyed method were immersed in laundry detergent for 10 min and then dried naturally. Almost no change of the morphology of resist-dyed Zn textile was observed (Figure S7,

Supporting Information), proving that Zn-active materials are strongly bonded on textile substrate.

This resist-assisted deposition method is able to convert the wavy fabric into cloth with arbitrary conductive patterns and different colors, which could be promising for applications in textile circuits and energy textiles. For demonstration, a series of conductive drawings (a flower, a word "NANO", a filamentary serpentine design) were fabricated on a polyester fabric with Ni, Cu, Zn, and NiCo BOH coatings, as shown in Figures 1f and S6. As conducting lines, a Cu textile was demonstrated to light commercial light-emitting diodes (LEDs) at flat and bended conditions (inset in Figure 1d). As current collectors of energy-storage textile, the textile electrodes can provide high-speed pathways for electron transport. Zn and NiCo BOH coatings can be subsequently applied as anode and cathode materials in micro-ZBs, respectively (see Figure S8 for the size of the interdigitated battery design). The average transmittance of 57.5% for pristine textile changes to 3.3% with Ni and 3.1% with Cu coatings, respectively (Figure S6b). As the micro-AZB is thin (0.1 mm, see Figure 1h), the device maintains the mechanical flexibility of pristine textiles, as confirmed by a bended textile micro-AZB in Figure 1g.

Though many printing methods can also produce desired patterns on textiles, our resist-dyeing process, compared with previously reported printing methods, has the following advantages. (1) Generally, the printing process, including screen printing and inkjet printing, involves toxic organic solvents and polymer binders. Our proposed resist-dyeing textile involves electroless- and electrodeposition of active materials in aqueous solution. It is more environmentally friendly without organic binders. (2) The organic binders typically make the textile rigid and uncomfortable, whereas the resist-dyed textile electrodes have excellent flexibility (Figure 1e). (3) The resist-dyed textile electrode has higher conductivity (Figure S6a). (4) The resist-dyed electrode has stronger bonding with the active coatings (Figure S7).
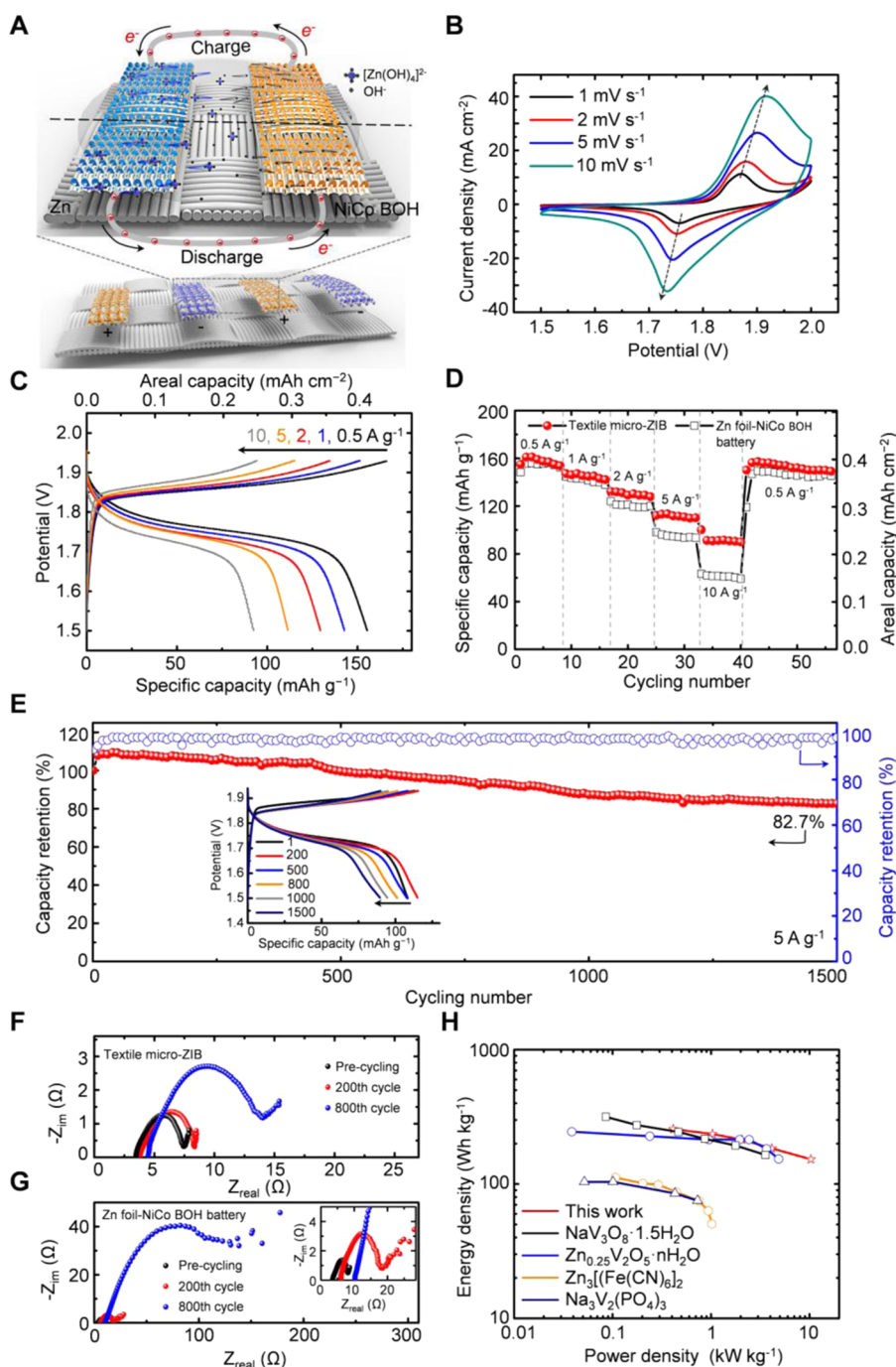
Figure 3. Electrochemical performances of the aqueous micro-AZBs. (A) Schematic illustration of the operation of textile micro-AZB during the charge−discharge processes. (B) Cyclic voltammetry (CV) profiles obtained at different scanning rates. (C) Galvanostatic charge−discharge (GCD) curves at different current densities. (D) Rate capability of the device at various current rates. (E) Cycling performance of the device at a current density of 5 A g^{-1}. (F, G) Nyquist plots of the Zn textile and Zn foil before cycling and after 200th and 800th cycles. (H) Ragone plot of the textile in comparison with other Zn batteries made of NaV$_3$O$_8$·1.5H$_2$O,[52] Zn$_{0.25}$V$_2$O$_5$·nH$_2$O,[48] Zn$_3$[Fe(CN)$_6$]$_2$,[49] and Na$_3$V$_2$(PO$_4$)$_3$.[51]
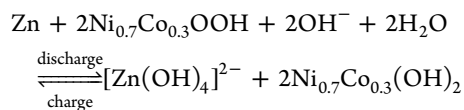
The Cu textile can be directly utilized as a current collector for flexible power sources due to the high electrical conductivity and flexibility. Vertically aligned ultrathin Zn nanosheets were grown on Cu fabrics as anode for micro-AZBs (Figure 2a). Freestanding Zn nanosheets were homogeneously grown on Cu films (Figure S9a,b). Importantly, each nanosheet is "rooted" in the Cu substrate, ensuring favorable pathways for electron transfers through the interface, as confirmed by the inset in Figures 2a, and S9c,d. Additionally, the cross-section SEM image and energy-dispersive X-ray

spectroscopy (EDS) elemental mapping of a Zn-coated Cu textile resolve the distribution of elemental C, O (from polyester backbone) and Ni, Cu, Zn (from metal coating), further confirming the uniform deposition of Zn nanosheets on the textile surface (see Figure 2b). The transmission electron microscopy (TEM) images in Figure 2c and high-resolution transmission electron microscopy (HRTEM) images in Figure 2d confirm the crystalline nature of the Zn nanosheets. The measured lattice fringe of 0.24 nm (inset in Figure 2d) is in accord with the (002) plane of hexagonal zinc (JCPDS #87-

0713). The crystallinity of Zn nanosheets is further confirmed by the X-ray diffraction (XRD) pattern (Figure 2e). The electroless deposited Ni is amorphous, but the Cu coating is crystalline, accounting for the high conductivity for the Cu textile substrate (Figure 1d). In addition, it is essential to ensure the stability of the polyester substrate in contact with various metal films via the aqueous plating method. Therefore, Fourier transform infrared (FTIR) spectra were employed (Figure 2f), where the existence of polyester can be identified from three characteristic peaks of 1710 cm^{-1} (asymmetric C=O stretching), 1243 cm^{-1} (C−O stretching), and 721 cm^{-1} (C−H bending).[40] Although the intensity is reduced due to the coating layers, the three characteristic peaks confirm the stability of the polyester substrate.

Ni−Co bimetallic oxyhydroxide was also electrodeposited on the Cu textile electrode as the cathode material. The reversible redox reaction between metallic oxyhydroxides and hydroxides has been applied in many supercapacitors. Better electrochemical performances of Ni−Co bimetallic oxyhydroxides over either Ni or Co oxyhydroxide have also been demonstrated.[41,42] According to the SEM images (Figure 2g), densely aligned ultrathin nanosheets were grown on the Cu-coated fibers, forming a uniform and porous film (Figure S9e). XPS spectra were further examined to confirm the formation of bimetallic oxyhydroxides. Besides two satellite peaks (noted as "sat."), the Ni 2p XPS spectrum shows two typical peaks located at 856.8 and 874.5 eV, in accordance with the Ni $2p_{3/2}$ and Ni $2p_{1/2}$ in nickel oxyhydroxide, respectively[41] (Figure 2h). Co 2p can be indexed at 781.9 eV (Ni $2p_{3/2}$) and 797.6 eV (Ni $2p_{1/2}$), in accordance with cobalt oxyhydroxide as well (Figure 2h).[43] The two peaks of the O 1s spectrum located at 531.2 and 533 eV suggest the O species in OH groups and absorbed water molecules, respectively[43,44] (Figure S9f). According to the atomic ratio by XPS data, the stoichiometrical chemical formula of the oxyhydroxide is determined to be $(Ni_{0.7}Co_{0.3})OOH$.

Electrochemical performances of textile electrodes and micro-AZBs were first performed in aqueous electrolyte. Figure S10 presents cyclic voltammetry (CV) curves of the textile Zn and $(Ni_{0.7}Co_{0.3})OOH$ electrode at a scan rate of 0.5 mV s^{-1} with a saturated calomel electrode (SCE) as the reference electrode. The full-cell reaction of a Zn−NiCo BOH battery can be written as

$$Zn + 2Ni_{0.7}Co_{0.3}OOH + 2OH^- + 2H_2O$$
$$\underset{charge}{\overset{discharge}{\rightleftharpoons}} [Zn(OH)_4]^{2-} + 2Ni_{0.7}Co_{0.3}(OH)_2$$

During the discharging process, the Zn nanosheets are oxidized to Zn^{2+} ions, which further combine with OH$^-$ in the electrolyte to form zincate ions ($[Zn(OH)_4]^{2-}$). Meantime, the bimetallic oxyhydroxide is reduced to bimetallic hydroxide at the cathode side. As for the charging process, the redox reactions are reversibly reversed, as schematically shown in Figure 3A.

For the fabrication of the micro-AZB full cell, the Zn anode was oversaturated, and the theoretical capacity ratio of the Zn anode to the NiCo BOH cathode was estimated to be about ~4. Therefore, current densities, specific capacities, and energy/power densities were all calculated based on the weight of cathode materials NiCo BOH. The aqueous electrolyte contains 1 M KOH, 0.02 M Zn(Ac)$_2$, 0.005 M LiOH, and 0.005 M Ca(OH)$_2$. The additives of Zn(Ac)$_2$,

LiOH, and Ca(OH)$_2$ can induce zincate supersaturation and enhance the rechargeability of NiCo BOH by suppressing O$_2$ evolution, potentially enhancing the cycling stability of the Zn−NiCo BOH battery.[10] Figure 3B shows cyclic voltammetry (CV) curves of micro-AZBs in aqueous electrolyte at different scanning rates. The two pairs of redox peaks are consistent with the two voltage plateaus in the charge−discharge curves shown in Figure 3C. A high discharge voltage of 1.7−1.8 V was obtained. When the charge−discharge current densities increase from 0.5, 1, 2, and 5 to 10 A g^{-1}, the discharge capacities of micro-AZBs decrease from 161.1, 145.5, 131.8, and 111.8 to 90.5 mAh g^{-1}, respectively, much higher than Zn foil−NiCo BOH battery assembled by stacking Zn foil and oxyhydroxide textile (dramatically dropping from 156.1 to 60.2 mAh g^{-1}, Figure 3D). This suggests the higher power performances of textile interdigitated micro-AZBs over the stacking-structured Zn foil-based batteries. The areal capacity of the device is about 0.41 mAh cm^{-2} at charge−discharge current density of 0.5 A g^{-1} (1.25 mA cm^{-2}) (Figure 3D). This areal capacity is better than or comparable to that of Zn/Ag batteries (0.19 mAh cm^{-2}),[45] Zn/Ni batteries (0.35 mAh cm^{-2}),[22] and Zn/V$_2$O$_5$ batteries (0.544 mAh cm^{-2})[46] but smaller than that of an all-printed Zn−Ag$_2$O battery (2.5 mAh cm^{-2}) due to its higher areal mass loading.[15]

The cycling performances of the Zn foil−NiCo BOH batteries and textile micro-AZBs at 5 A g^{-1} were compared in aqueous electrolyte (Figure S11). The micro-AZBs exhibited stable cycling for over 1500 cycles with capacity retention of 82.7% (Figure 3E), whereas the Zn foil−NiCo BOH battery showed 20.3% capacity decay after only 800 cycles (Figure S11a). Throughout the course of cycling, the charging−discharging profiles are stable without significantly increased polarization (the inset of Figure 3E). In addition, AC impedance spectra of the textile micro-AZBs after 800 cycles show much smaller increase in the electrolyte resistance (R_s) and about an order lower charge-transfer resistance (R_{ct}) than that of the Zn foil-based battery, as shown in Figure 3F,G. The unstable cycling performances and quickly increased internal impedance of the Zn foil−NiCo BOH battery are ascribed to the dramatic dendrite growth and the formation of less reversible and less conductive Zn oxide/hydroxide at the anode side,[47] which will be further discussed in the following sections. In addition, we also conducted experiments to compare the electrochemical performance of two different Zn textile (screen-printing Zn textile and resist-dyed Zn textile) batteries. CV and GCD curves of the resist-dyed Zn textile batteries show much smaller charge−discharge overpotentials and higher discharge capacities (Figure S12) than that of the screen-printed Zn textile battery mainly due to the above-discussed higher conductivity of the electrode.

Table S1 compares the energy density and power density of NiCo BOH obtained in this work with previously reported various cathode materials of Zn batteries. As shown by the Ragone plot (Figure 3H), the highest energy density of our textile micro-AZBs was estimated to be 256.2 Wh kg^{-1}, which is higher than that of steel mesh-based Zn/Zn$_{0.25}$V$_2$O$_5$ batteries (≈250 Wh kg^{-1}),[48] Zn/Zn$_3$[Fe(CN)$_6$]$_2$ batteries (≈100 Wh kg^{-1}),[49] Zn/Co$_3$O$_4$ batteries fabricated on carbon cloth (≈241 Wh kg^{-1}),[47] and Zn/LiMn$_2$O$_4$ batteries on porous carbon (≈180 Wh kg^{-1})[50] and is also comparable to that of Zn/MnO$_2$ batteries on CNT paper substrate (≈254 Wh kg^{-1})[24] and NiSn/LiMnO$_2$ microbatteries[33] directly grown on glass slides (Table S1). The power density of the textile Zn microbatteries
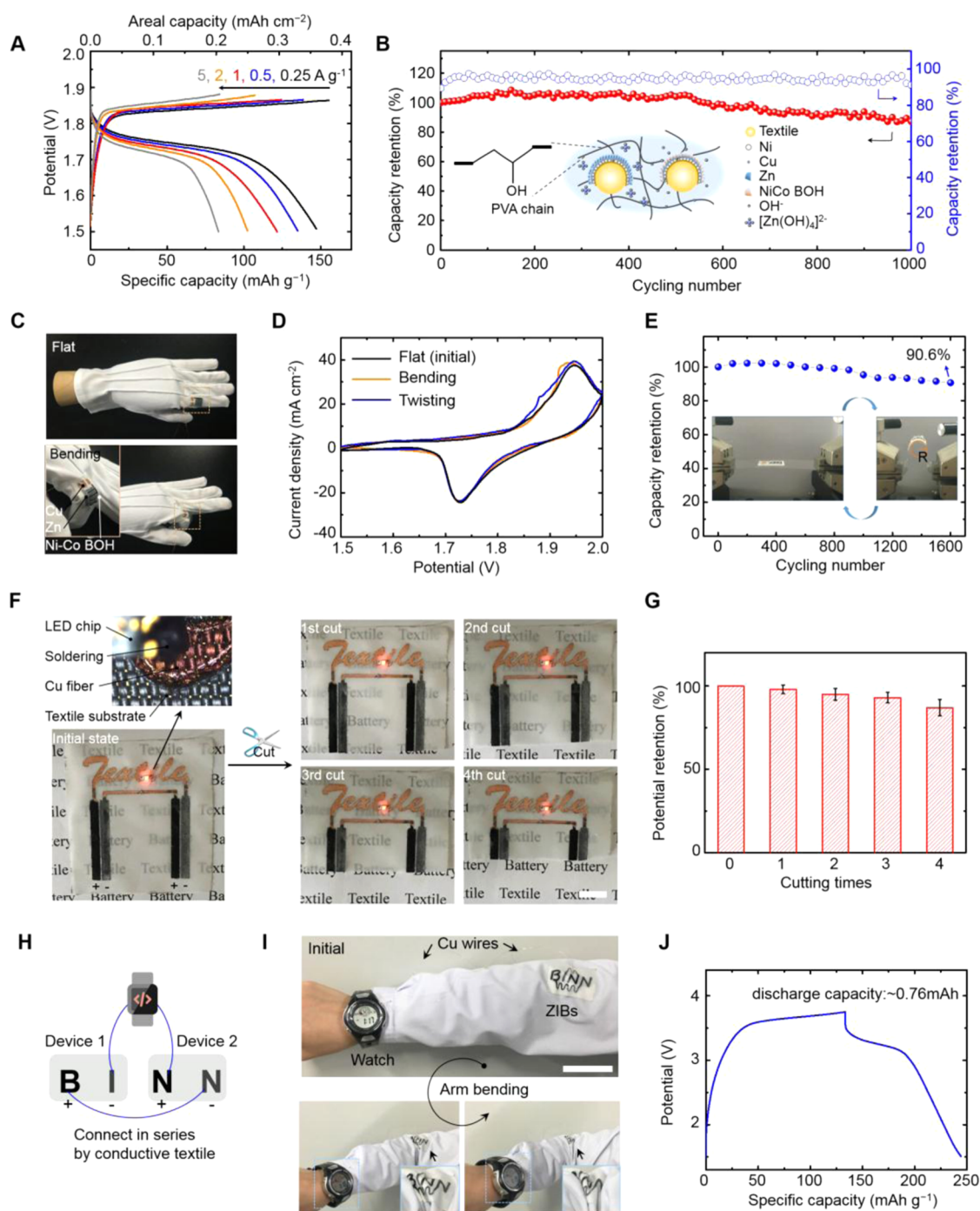
Figure 4. Electrochemical performances and mechanical properties of solid-state textile micro-AZBs. (A) GCD curves of the device at various current densities. (B) Cycling performance of the micro-AZB at a current density of 2.5 A g^{-1}. (C) Photos of a micro-AZB conformally attached on the glove of a bending finger. (D) CV curves at a scan rate of 10 mV s^{-1} recorded under flat, bending, and twisting conditions. (E) Capacity retention as a function of bending cycles. The radius of curvature R = 4.1 mm. (F) Cutting test of the textile AZBs. The LED cells can still be powered through the letter ("textile")-shaped Cu textile circuit after the first, second, third, and fourth cuts of AZBs. (G) Potential retention of the AZB at different cutting statuses. (H) AZBs in the shape of four letters, that is, "BINN". The letter-shaped AZBs sewed on a garment power a commercial watch under bending condition. (J) GCD curves of the BINN AZBs. Scale bar, 1 cm (F) and 5 cm (I).

reached 10.3 kW kg^{-1}, generally much higher than most previously reported Zn batteries (0.51−8.66 kW kg^{-1}).[22,49,51−54] The total specific capacity and energy density of the device even considering the weight of Ni/Cu metal layers (3.1 mg cm^{-2}) are 70.6 mAh g^{-1} and 114.3 Wh kg^{-1} (0.5 A g^{-1}), respectively. The high electrochemical performances of our device are attributed to the following factors: (1)

ultrathin nanosheets of Zn and oxyhydroxides rooted in the highly conductive Cu films favor the high-speed transfer of electrons; (2) the porous morphology and large surface area of active materials at both electrodes reduce the electrolyte/ electrode impedance; and (3) the advantage of the in-plane interdigitated configuration.
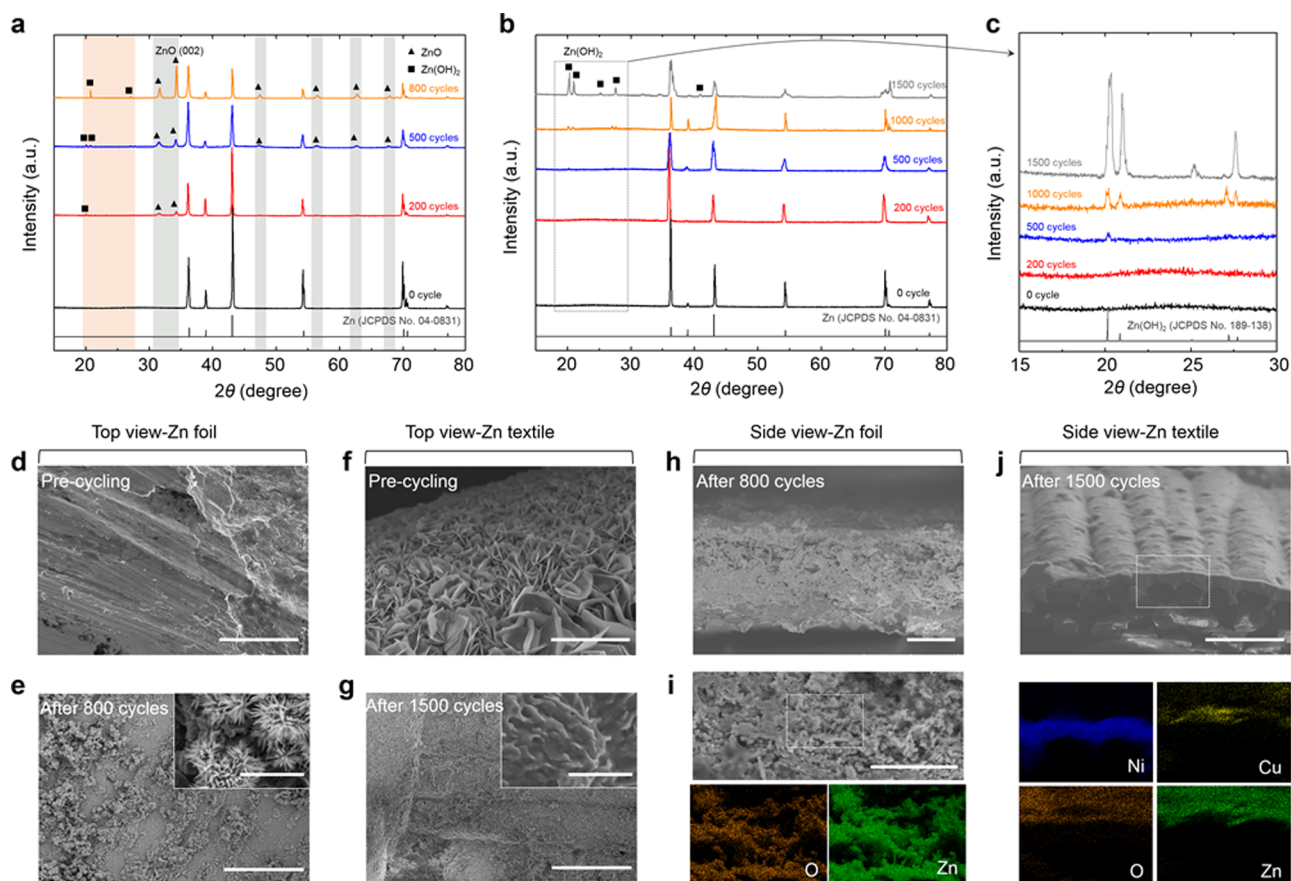
Figure 5. Cycling performance of Zn electrode. XRD pattern of Zn foil (a) and Zn textile (b,c) electrodes during cycling. Top-view SEM images show the morphology of Zn foil before (d) and after (e) cycling. Top-view SEM analysis of Zn textile before (f) and after (g) cycling. Cross-section SEM images and their corresponding EDS elemental mapping of side view of the Zn foil (h, i) after 800 cycles and Zn textile (j) electrode after 1500 cycles. Scale bars, 5 μm (d, f), 50 μm (e, g–j), and 1 μm (inset of (e, g)).

The solid-state micro-AZB was fabricated by coating interdigitated textile electrodes with a poly(vinyl alcohol) (PVA) gel-type electrolyte. The specific discharge capacities of solid micro-AZB at 0.25, 0.5, 1, 2, and 5 A g^{-1} were 147.2, 135.1, 121.6, 102.4, and 83.5 mAh g^{-1}, respectively (Figure 4A). The specific areal discharge capacities of solid micro-AZB at 0.625, 1.25, 2.5, 5, and 12.5 mA cm^{-2} were 0.36, 0.33, 0.30, 0.25, and 0.21 mAh cm^{-2}, respectively (Figure 4A). Compared to the above aqueous micro-AZB, these specific capacities decrease slightly, but are still better than or comparable to several representative studies on solid-state Zn batteries.[20] The cycling stability of solid micro-AZBs was further studied at 2.5 A g^{-1} (Figure 4B). Excellent capacity retention of 87.2% was obtained even after 1000 deep cycles.

Mechanical durability is essential for wearable applications; therefore, the flexibility of the textile micro-AZB has been examined under various deformation conditions. The soft textile micro-AZBs attached on a glove can be easily bended and twisted (Figure 4C). The CV curves tested in situ at deformed states show no obvious change compared to the initial state (Figure 4D). The device was then bent for 1600 cycles by a linear motor (the inset photos in Figure 4E). After the bending cycles, only 9.4% capacity decay was observed, as shown in Figure 4E. A red LED can still be lighted by the textile micro-AZB even at deformed state (Figure S13). These tests confirm the excellent flexibility of the solid micro-AZBs, which is mainly attributed to the flexible textile substrate and

the intimate and strong binding between coating materials (Ni, Cu, Zn, and oxyhydroxide) and fiber surfaces.

Tailoring is usually required for cloth designs, so a self-powered illuminating textile was designed for demonstration of the tailoring ability of the textile micro-AZB (see Figure 4F). Two in-plane AZBs were fabricated and connected in series by a letter-shaped Cu textile circuit, on which a red LED chip was soldered. The LED can be lighted by the textile AZBs under bending or twisting deformation (Movie S1). It is noteworthy that the AZB can also power the LED after four times of cutting by a scissor (Figures 4F and S13c,d). The open-circuit voltage of the AZBs shows only slight decrease after four cuttings (87% of its initial value), suggesting a negligible current leakage during the tailoring process (Figure 4G). These results demonstrate that our solid-state AZB can serve as a tailorable energy-storing textile.

The resist-dyeing-based fabrication of our micro-AZBs is facile to convert drawings, paintings, or letters on a cloth into energy textiles. For demonstration, we designed two AZBs on a polyester fabric in the form of four letters (BINN). The two AZBs ("BI" is one device and "NN" is the other one) were connected in series (Figures 4H and S13f). The devices can be easily sewed onto a cloth (Figure 4I) and power an electronic watch under bending condition. The watch kept operating even when the energy textile was repeatedly bended by casual arm motions (Movie S2). The representative GCD profiles of this letter-shaped battery are provided in Figure 4J, showing a
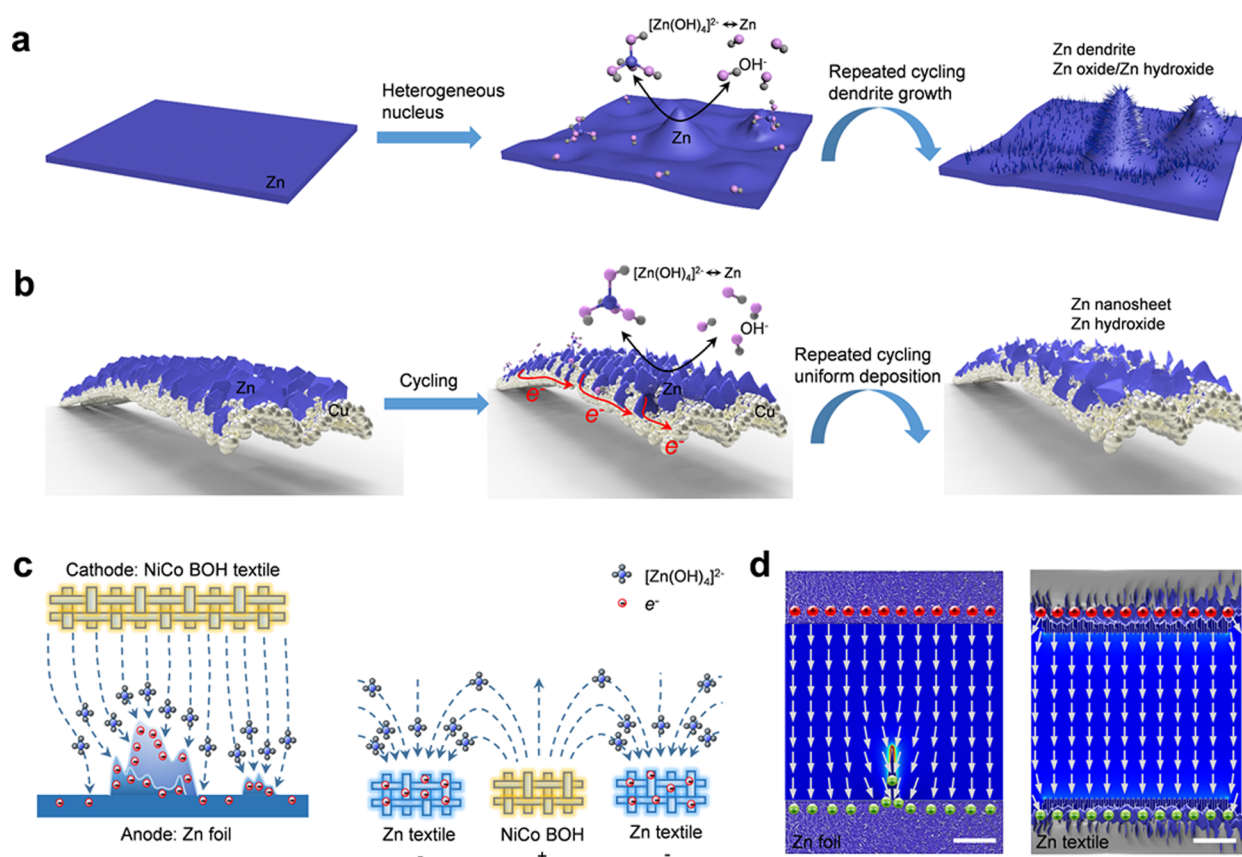
Figure 6. Scheme of the deposition behaviors of Zn electrodes. Schematic illustrates the morphologies of Zn deposited on Zn foil (a, c) and Cu textile substrate (b, d) during cycling. The arrows in (c) indicate the distribution of electric field and the possible site where Zn would be preferentially deposited. (d) Simulated electric field distribution in Zn foil and Zn textile electrodes. Scale bar, 10 μm.

~3.3 V discharge voltage plateau and a discharge capacity of 0.76 mAh. More complicated images, drawings, or letters could also be designed into comfortable and aesthetic energy textiles as long as desirable Kapton resist is designed for laser scribing.

The Zn metal anode typically suffers from issues of low reversibility, caused mainly by the Zn dendrite growth and irreversible side reactions. Zn/Zn symmetrical cells were assembled and tested to compare the reversibility of the Zn foil electrode and the textile Zn electrode in alkaline aqueous electrolyte. Figure S14 compares the cycling stability of screen-printed Zn textile with that of resist-dyed Zn textile in alkaline electrolyte. The screen-printed Zn textile electrode has a sharp increase in charge–discharge overpotentials after about 60 000 s, whereas the resist-dyed textile electrode shows relatively more stable performances. Figure S15 shows a comparison of voltage hysteresis and cycling stability of Zn foil and Zn textile symmetric cell in aqueous electrolyte, respectively. At a current density of 1 mA cm^{-2}, both cells exhibited similar initial potential, but a sudden increase in polarization of the Zn foil symmetric cell was observed after cycling for about 77 000 s. Dramatic increase in polarization of the Zn foil cell was even observed readily after only several cycles at 3 mA cm^{-2}. In contrast, Zn textile symmetric cells show stable voltage profiles without significant polarization. Typically, heterogeneous Zn dendrite growth and formation of Zn oxide/hydroxide are ascribed to the large polarization of the Zn metal electrode during cycling.[20]
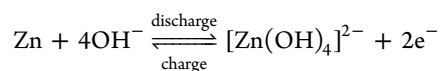
To understand these issues, ex situ XRD was examined for Zn anodes of both aqueous Zn foil–NiCo BOH battery and

textile micro-AZB at charged state after cycling. After only 200 cycles, peaks of $Zn(OH)_2$ and ZnO can be observed in the Zn foil electrode (Figure 5a). The peak intensity of $Zn(OH)_2$/ ZnO keeps increasing after 500 and 800 cycles, suggesting more Zn was continuously transformed into insulating byproducts along with the cycling. After 800 cycles, the intensity of $ZnO(002)$ peak is comparable to most Zn peaks, indicating a thick ZnO layer formed on the Zn foil. In contrast, no obvious peak of $Zn(OH)_2$ is identified in the Zn textile electrode until 1000 cycles (Figure 5b,c). After 1500 cycles, the peaks of $Zn(OH)_2$ are noticeable, but throughout the course of cycling, no obvious peak of ZnO is observed. During the cycling, the zincates $(Zn(OH)_4)^{2-}$ and $Zn(OH)_2$ can transform to ZnO through a dehydration reaction. Ideally, the ZnO or $Zn(OH)_2$ can be reduced again into Zn and deposit on the anode, as suggested by several previous reports.[10,47] However, the observed $ZnO/Zn(OH)_2$ here at charged state indicates that they have not been converted back to Zn and are no longer reversible or electrochemical active. These irreversible byproducts consume the active material of Zn metal and also deteriorate cell kinetics due to their insulating nature. Compared with the Zn foil, side reactions are largely delayed and the reversibility is significantly improved for the textile Zn electrode.

SEM images of charged Zn electrodes after cycling in aqueous electrolyte were also taken to understand the morphology evolution. The smooth top surface of the initial Zn foil (Figure 5d) changes to be highly rough with lots of aggregated bumps of needlelike Zn dendrites after 500 and 800

cycles (see Figures S16a and 5e, respectively), whereas the initial Zn nanosheets on fabric fibers (Figure 5f) change into a smooth and uniform film without noticeable Zn dendrite after even 1500 cycles (Figures 5g, S16b and S18). The side-view SEM image of the Zn foil after 800 cycles exhibits a porous and pulverized morphology (Figure 5h,i). At higher magnifications (Figure S17), the deposited Zn during the cycling shows a cactuslike hierarchical morphology with many Zn nanoneedles. In contrast, dense and conformal Zn film on fabric fibers is observed for the textile Zn electrode after 1500 cycles (Figure 5j). The EDS mapping confirms the existence of ZnO/ $Zn(OH)_2$ (Figure 5i,j).

The morphology evolution of Zn foil and Zn textile during cycling can be schematically explained in Figure 6. The electrochemical reaction of the Zn anode in alkaline electrolyte is shown as the following equation[10,47]

$$Zn + 4OH^- \underset{\text{charge}}{\overset{\text{discharge}}{\rightleftharpoons}} [Zn(OH)_4]^{2-} + 2e^-$$

The electro-oxidation of Zn leads to the stripping of zincate ions from the substrate, which can be reduced and electrodeposited back to the surface when the applied external current is reversed. During the electrodeposition process, the freshly formed Zn prefers the surfaces of formerly nucleated Zn particles due to the lower surface energy and shorter ion diffusion distances. Meantime, the electric field between the anode and cathode will concentrate at the dendrite tip sites, which amplifies the local growth of dendrite due to concentrated ions and electrons at the electrode–electrolyte interfaces (Figure 6c).[55,56] Simulation of the electric field distribution generated in Zn foil and Zn textile is depicted in Figure 6d. An electric field enhancement occurs at the dendrite tip of Zn foil, which results in charge buildup. This is due to the lightning-rod effect of the sharp geometry.[57] The electric field is driven out of the top electrode and will converge at the convex part of the interface. The increase in the magnitude of the electric field will dramatically amplify the Zn dendrite growth rate.[55] The repeated stripping/depositing of Zn along with cycling then leads to the pulverization of Zn and heterogeneous growth of hierarchical dendrites, which, together with the above-observed byproduct layers, result in the dramatically increased impedance, worse cycling performances, and possibly internal short-circuit hazard.

Compared with the flat Zn foil electrode, Zn nanosheets standing on numerous microfibers of porous fabrics can supply much larger effective surface areas. The surface of each ultrathin nanosheet is a preferable site for freshly electrodeposited Zn during the charging process (Figure 6b). The electric field tends not to be locally concentrated due to the parallel configuration of finger electrodes and the nanoscale porous structures of active materials (Figure 6c). High-density Zn nanosheets will disperse the concentrated electric field, and the electric field will be relatively uniform with no strong electric field enhancement (Figure 6d). Therefore, the repeated Zn deposition is much more homogeneous and the dendrite growth is significantly suppressed.

■ CONCLUSIONS

In summary, we have developed a versatile approach to fabricating textile-based energy-storage devices with the inspiration from traditional resist-dyeing techniques. Owing to the wavy surface and porous morphology of fabrics, most

lithography and coating methods are inapplicable; however, desired patterns can be prepared on textile substrates by a variety of dyeing techniques. By combining resist-dyeing and electroless/electrodeposition methods, arbitrary conductive patterns (Ni, Cu, or Zn) were realized on textiles. Our methods also allow the fabrication of coplanar micro-AZBs (Zn–NiCo BOH) on a single fabric, which showed mainly the following advantages: (1) high energy/power densities, (2) excellent tailoring ability and flexibility of gel electrolyte-based solid-state micro-AZBs, (3) capability in designing AZBs into arbitrary drawings or letters, and importantly (4) high reversibility and long-term cycling stability due to the significantly suppressed Zn dendrite growth and side reactions. Compared with other printing methods, our resist-dyed electrodes also have better conductivity, flexibility, and higher electrochemical performances. The ideal power source for electronic textile should be in the form of textile as well. Our proposed textile micro-AZBs, combining the advantages of high energy density and high safety with minimal sacrifice in the soft/comfort/stylish requirements of fabrics, have great promise in powering e-textiles or wearable electronics.

■ EXPERIMENTAL METHODS

Fabrication of Patterned Conductive Textile. Polyester or nylon textile was carefully cleaned by ethanol and deionized (DI) water in an ultrasonic bath for 40 min. Subsequently, the textile was sealed with a Kapton mask patterned by a laser scribing system. Ni was then deposited on the textile substrate by the electroless plating method similar to our previous report.[58] Cu was subsequently deposited on the previous fabricated Ni film in a 0.1 M $CuSO_4$ aqueous solution for 5, 10, and 15 min with a piece of Cu plate as the counter electrode and the reference electrode. The pH was adjusted to ~10 by 10% NaOH solution. After peeling off the Kapton mask, the Cu cloth was washed with deionized (DI) water and then dried in a vacuum oven. For 10 min electrodeposition of Cu, the final Ni/Cu metal layer has an areal weight of ~3.1 mg cm^{-2}.

Fabrication of Zn Anode and CoNi BOH Cathode. Zn nanosheets were coated on top of the Cu textile (10 min deposition) by electrodeposition under −0.9 V in an aqueous solution containing 0.2 M $ZnSO_4 \cdot 7H_2O$ and 0.5 M $Na_3C_6H_5O_7 \cdot 2H_2O$ for 5 min using a piece of Zn plate as the counter electrode and the reference electrode. After electrodeposition of the Zn anode, the sample was carefully rinsed with deionized water and dried in air. The sample was put in an aqueous solution containing 0.1 M $NiSO_4 \cdot 6H_2O$, 0.1 M $Co(NO_3)_2 \cdot 6H_2O$, and 0.5 M Na_2SO_4 for the electrodeposition of NiCo BOH on the other finger electrode of the interdigitated Cu film. The NiCo BOH coating experiment was performed under −1 V for 10 min in a standard three-electrode cell with a piece of Pt plate counter electrode and SCE reference electrode. On average, about 2.9 mg cm^{-2} of Zn and about 2.5 mg cm^{-2} of NiCo BOH active materials were grown on Cu textile electrodes. Considering the theoretical capacities of NiCo BOH positive electrode (242 mAh g^{-1})[41] and Zn negative electrode (819 mAh g^{-1}),[20] the theoretical capacity ratio of negative to positive electrode is about ~4. All the specific capacities, energy densities, and power densities were calculated based on the weight of cathode materials NiCo BOH. Finally, the sample was then washed with DI water and dried in a vacuum oven. The width and the interspace of the Zn and NiCo BOH microelectrodes were 7.9 mm and 0.4 mm, respectively. The total area of the device was estimated to be 1.07 cm^{-2}.

Fabrication of Textile Solid-State Micro-AZBs. The aqueous electrolyte consists of 1 M KOH, 0.02 M $Zn(Ac)_2$, and 0.005 M LiOH and $Ca(OH)_2$. Polymeric gel electrolytes were prepared by stirring 10 mL of DI water and 1.0 g of PVA (M_w 89 000−98 000) into the above fabricated aqueous electrolyte at 85 °C for 1 h. About 0.3 mL of the electrolyte was dropped to the active area of the device and was then dried at room temperature.

Characterizations. The electrochemical performance was measured by an electrochemical work station (CHI 760E). The CV curves of the textile Zn electrode and the NiCo BOH electrode were separately measured at 0.5 mV s^{-1} in a standard three-electrode cell consisting of a piece of Pt plate counter electrode, an SCE reference electrode, and 1 M KOH and 0.02 M Zn(Ac)$_2$ aqueous electrolyte. The aqueous electrolyte used for all full cells is 1 M KOH, 0.02 M Zn(Ac)$_2$, 0.005 M LiOH, and 0.005 M Ca(OH)$_2$. The CV of Zn−NiCo BOH full cell was measured at different scanning rates between 1.5 and 2.0 V. The GCD cycling values of Zn−NiCo BOH aqueous cells and solid-state cells were tested by a battery cycler (LAND CT2001A) at different current densities. The current density, specific capacity, and energy/power density were all calculated based on the weight of NiCo BOH at the cathode side. Electrochemical impedance spectroscopy was measured by AUTOLAB PGSTAT302N in the frequency range of 0.1 Hz−100 kHz with 5 mV voltage amplitude. SEM images were taken with a Hitachi SU8020. TEM images were characterized using a FEI TECNAI F20. XRD measurements were performed by a PANalytical instrument (X'Pert 3 Powder). The UV−vis spectra were obtained by a Shimadzu UV-3600 spectrometer, and XPS spectra were obtained by ESCALAB 250Xi. FTIR spectra were taken by Bruker/VERTEX80v, and the optical microscopy images were taken by an Axio Imager.M2m. A step motor (Linmot E1100) was used to test the mechanical stability of the device.

Numerical Simulation. Finite element method was employed to predict the electric field distribution in different simulation cases. The simulation was performed by employing an electrical conduction model[59] to simplify the experiment. Zn foil model and Zn textile model were constructed with a fixed distance of 50 μm between the two electrodes. A potential of 1.5 V was applied. The magnitude of the electric field and its vector distribution were studied.

■ ASSOCIATED CONTENT

ⓢ Supporting Information

The Supporting Information is available free of charge on the ACS Publications website at DOI: 10.1021/acsami.8b19825.

> Schematic illustration of resist-dyeing fabrication of patterned textiles; optical microscope image, contact angle tests, and SEM image of the patterned textile; dimensions of the device; morphology and structure characterization of Zn and NiCo BOH textile electrode; CV curves of the Zn and NiCo BOH textile electrode in aqueous electrolyte; cycling comparison of Zn foil and Zn textile AZBs; SEM, CV, and GCD curves of screen-printing Zn textile battery and resist-dyed Zn textile battery; mechanical durability and cutting tests of the device; Zn−Zn symmetric cells with Zn foil and Zn textile electrodes; SEM image of Zn foil and Zn textile after cycling; side-view SEM images of Zn foil with increasing magnification after 800 cycles; SEM images and EDS elemental mapping of the Zn textile after cycling (PDF)
>
> Bendability of textile micro-ZIBs (AVI)
>
> Watch can be powered by the letter-shaped Zn textile batteries at bended state (AVI)

■ AUTHOR INFORMATION

Corresponding Authors
*E-mail: puxiong@binn.cas.cn (X.P.).
*E-mail: huweiguo@binn.cas.cn (W.H.).
*E-mail: zlwang@gatech.edu (Z.L.W.).

ORCID Ⓘ
Xiong Pu: 0000-0002-1254-8503
Zhixiao Liu: 0000-0002-5354-4701
Weiguo Hu: 0000-0002-8614-0359

Zhong Lin Wang: 0000-0002-5530-0380

Notes

The authors declare no competing financial interest.

■ ACKNOWLEDGMENTS

■ REFERENCES

(1) Wu, W.; Wen, X.; Wang, Z. L. Taxel-Addressable Matrix of Vertical-Nanowire Piezotronic Transistors for Active and Adaptive Tactile Imaging. *Science* **2013**, *340*, 952−957.

(2) Wang, C.; Wang, C.; Huang, Z.; Xu, S. Materials and Structures toward Soft Electronics. *Adv. Mater.* **2018**, No. 1801368.

(3) Pan, C.; Dong, L.; Zhu, G.; Niu, S.; Yu, R.; Yang, Q.; Liu, Y.; Wang, Z. L. High-resolution electroluminescent imaging of pressure distribution using a piezoelectric nanowire LED array. *Nat. Photonics* **2013**, *7*, 752−758.

(4) Zhang, Z.; Cui, L.; Shi, X.; Tian, X.; Wang, D.; Gu, C.; Chen, E.; Cheng, X.; Xu, Y.; Hu, Y.; Zhang, J.; Zhou, L.; Fong, H. H.; Ma, P.; Jiang, G.; Sun, X.; Zhang, B.; Peng, H. Textile Display for Electronic and Brain-Interfaced Communications. *Adv. Mater.* **2018**, *30*, No. 1800323.

(5) Hua, Q.; Sun, J.; Liu, H.; Bao, R.; Yu, R.; Zhai, J.; Pan, C.; Wang, Z. L. Skin-inspired highly stretchable and conformable matrix networks for multifunctional sensing. *Nat. Commun.* **2018**, *9*, No. 244.

(6) Liu, M.; Pu, X.; Jiang, C.; Liu, T.; Huang, X.; Chen, L.; Du, C.; Sun, J.; Hu, W.; Wang, Z. L. Large-Area All-Textile Pressure Sensors for Monitoring Human Motion and Physiological Signals. *Adv. Mater.* **2017**, *29*, No. 1703700.

(7) Kwak, S. S.; Kim, H.; Seung, W.; Kim, J.; Hinchet, R.; Kim, S.-W. Fully Stretchable Textile Triboelectric Nanogenerator with Knitted Fabric Structures. *ACS Nano* **2017**, *11*, 10733−10741.

(8) Wen, Z.; Yeh, M. H.; Guo, H.; Wang, J.; Zi, Y.; Xu, W.; Deng, J.; Zhu, L.; Wang, X.; Hu, C.; et al. Self-Powered Textile for Wearable Electronics by Hybridizing Fiber-Shaped Nanogenerators, Solar Cells, and Supercapacitors. *Sci. Adv.* **2016**, *2*, No. e1600097.

(9) Zeng, Y.; Meng, Y.; Lai, Z.; Zhang, X.; Yu, M.; Fang, P.; Wu, M.; Tong, Y.; Lu, X. An Ultrastable and High-Performance Flexible Fiber-Shaped Ni−Zn Battery based on a Ni−NiO Heterostructured Nanosheet Cathode. *Adv. Mater.* **2017**, *29*, No. 1702698.

(10) Parker, J. F.; Chervin, C. N.; Pala, I. R.; Machler, M.; Burz, M. F.; Long, J. W.; Rolison, D. R. Rechargeable nickel−3D zinc batteries: An energy-dense, safer alternative to lithium-ion. *Science* **2017**, *356*, 415−418.

(11) Xiao, X.; Li, T.; Yang, P.; Gao, Y.; Jin, H.; Ni, W.; Zhan, W.; Zhang, X.; Cao, Y.; Zhong, J.; Gong, L.; Yen, W.-C.; Mai, W.; Chen, J.; Huo, K.; Chueh, Y.-L.; Wang, Z. L.; Zhou, J. Fiber-Based All-Solid-State Flexible Supercapacitors for Self-Powered Systems. *ACS Nano* **2012**, *6*, 9200−9206.

(12) Ma, L.; Chen, S.; Pei, Z.; Li, H.; Wang, Z.; Liu, Z.; Tang, Z.; Zapien, J. A.; Zhi, C. Flexible Waterproof Rechargeable Hybrid Zinc Batteries Initiated by Multifunctional Oxygen Vacancies-Rich Cobalt Oxide. *ACS Nano* **2018**, *12*, 8597−8605.

(13) Wang, R.; Han, Y.; Wang, Z.; Jiang, J.; Tong, Y.; Lu, X. Nickel@Nickel Oxide Core−Shell Electrode with Significantly Boosted Reactivity for Ultrahigh-Energy and Stable Aqueous Ni−Zn Battery. *Adv. Funct. Mater.* **2018**, *28*, No. 1802157.

(14) Zeng, Y.; Lai, Z.; Han, Y.; Zhang, H.; Xie, S.; Lu, X. Oxygen-Vacancy and Surface Modulation of Ultrathin Nickel Cobaltite Nanosheets as a High-Energy Cathode for Advanced Zn-Ion Batteries. *Adv. Mater.* **2018**, *30*, No. 1802396.

(15) Kumar, R.; Shin, J.; Yin, L.; You, J.-M.; Meng, Y. S.; Wang, J. All-Printed, Stretchable Zn−Ag$_2$O Rechargeable Battery via Hyperelastic Binder for Self-Powering Wearable Electronics. *Adv. Energy Mater.* **2017**, 7, No. 1602096.

(16) Nam, G.; Park, J.; Choi, M.; Oh, P.; Park, S.; Kim, M. G.; Park, N.; Cho, J.; Lee, J.-S. Carbon-Coated Core−Shell Fe−Cu Nanoparticles as Highly Active and Durable Electrocatalysts for a Zn−Air Battery. *ACS Nano* **2015**, 9, 6493−6501.

(17) Yu, M.; Wang, Z.; Hou, C.; Wang, Z.; Liang, C.; Zhao, C.; Tong, Y.; Lu, X.; Yang, S. Nitrogen-Doped Co3O4 Mesoporous Nanowire Arrays as an Additive-Free Air-Cathode for Flexible Solid-State Zinc−Air Batteries. *Adv. Mater.* **2017**, 29, No. 1602868.

(18) Zhu, L.; Zheng, D.; Wang, Z.; Zheng, X.; Fang, P.; Zhu, J.; Yu, M.; Tong, Y.; Lu, X. A Confinement Strategy for Stabilizing ZIF-Derived Bifunctional Catalysts as a Benchmark Cathode of Flexible All-Solid-State Zinc−Air Batteries. *Adv. Mater.* **2018**, 30, No. 1805268.

(19) Chen, X.; Liu, B.; Zhong, C.; Liu, Z.; Liu, J.; Ma, L.; Deng, Y.; Han, X.; Wu, T.; Hu, W.; Lu, J. Ultrathin Co3O4 Layers with Large Contact Area on Carbon Fibers as High-Performance Electrode for Flexible Zinc−Air Battery Integrated with Flexible Display. *Adv. Energy Mater.* **2017**, 7, No. 1700779.

(20) Pan, H.; Shao, Y.; Yan, P.; Cheng, Y.; Han, K. S.; Nie, Z.; Wang, C.; Yang, J.; Li, X.; Bhattacharya, P.; Mueller, K. T.; Liu, J. Reversible aqueous zinc/manganese oxide energy storage from conversion reactions. *Nat. Energy* **2016**, 1, No. 16039.

(21) Tikekar, M. D.; Archer, L. A.; Koch, D. L. Stabilizing electrodeposition in elastic solid electrolytes containing immobilized anions. *Sci. Adv.* **2016**, 2, No. e1600320.

(22) Liu, J.; Guan, C.; Zhou, C.; Fan, Z.; Ke, Q.; Zhang, G.; Liu, C.; Wang, J. A Flexible Quasi-Solid-State Nickel-Zinc Battery with High Energy and Power Densities Based on 3D Electrode Design. *Adv. Mater.* **2016**, 28, 8732−8739.

(23) Li, M.; Meng, J.; Li, Q.; Huang, M.; Liu, X.; Owusu, K. A.; Liu, Z.; Mai, L. Finely Crafted 3D Electrodes for Dendrite-Free and High-Performance Flexible Fiber-Shaped Zn−Co Batteries. *Adv. Funct. Mater.* **2018**, 28, No. 1802016.

(24) Li, H.; Han, C.; Huang, Y.; Huang, Y.; Zhu, M.; Pei, Z.; Xue, Q.; Wang, Z.; Liu, Z.; Tang, Z.; Wang, Y.; Kang, F.; Li, B.; Zhi, C. An extremely safe and wearable solid-state zinc ion battery based on a hierarchical structured polymer electrolyte. *Energy Environ. Sci.* **2018**, 11, 941−951.

(25) Liu, L.; Yu, Y.; Yan, C.; Li, K.; Zheng, Z. Wearable energy-dense and power-dense supercapacitor yarns enabled by scalable graphene−metallic textile composite electrodes. *Nat. Commun.* **2015**, 6, No. 7260.

(26) Song, Y.; Chen, H.; Chen, X.; Wu, H.; Guo, H.; Cheng, X.; Meng, B.; Zhang, H. All-in-one piezoresistive-sensing patch integrated with micro-supercapacitor. *Nano Energy* **2018**, 53, 189−197.

(27) Chai, Z.; Zhang, N.; Sun, P.; Huang, Y.; Zhao, C.; Fan, H. J.; Fan, X.; Mai, W. Tailorable and Wearable Textile Devices for Solar Energy Harvesting and Simultaneous Storage. *ACS Nano* **2016**, 10, 9201−9207.

(28) Yu, M.; Lin, D.; Feng, H.; Zeng, Y.; Tong, Y.; Lu, X. Boosting the Energy Density of Carbon-Based Aqueous Supercapacitors by Optimizing the Surface Charge. *Angew. Chem.* **2017**, 129, 5546−5551.

(29) Balogun, M.-S.; Qiu, W.; Lyu, F.; Luo, Y.; Meng, H.; Li, J.; Mai, W.; Mai, L.; Tong, Y. All-flexible lithium ion battery based on thermally-etched porous carbon cloth anode and cathode. *Nano Energy* **2016**, 26, 446−455.

(30) Zhang, Y.; Zhao, Y.; Ren, J.; Weng, W.; Peng, H. Advances in Wearable Fiber-Shaped Lithium-Ion Batteries. *Adv. Mater.* **2016**, 28, 4524−4531.

(31) Duan, J.; Xie, W.; Yang, P.; Li, J.; Xue, G.; Chen, Q.; Yu, B.; Liu, R.; Zhou, J. Tough hydrogel diodes with tunable interfacial adhesion for safe and durable wearable batteries. *Nano Energy* **2018**, 48, 569−574.

(32) Liu, Y.; Liu, Q.; Zhang, A.; Cai, J.; Cao, X.; Li, Z.; Asimow, P. D.; Zhou, C. Room-Temperature Pressure Synthesis of Layered Black

Phosphorus−Graphene Composite for Sodium-Ion Battery Anodes. *ACS Nano* **2018**, 12, 8323−8329.

(33) Pikul, J. H.; Gang Zhang, H.; Cho, J.; Braun, P. V.; King, W. P. High-power lithium ion microbatteries from interdigitated three-dimensional bicontinuous nanoporous electrodes. *Nat. Commun.* **2013**, 4, No. 1732.

(34) Park, M.; Im, J.; Shin, M.; Min, Y.; Park, J.; Cho, H.; Park, S.; Shim, M.-B.; Jeon, S.; Chung, D.-Y.; Bae, J.; Park, J.; Jeong, U.; Kim, K. Highly stretchable electric circuits from a composite material of silver nanoparticles and elastomeric fibres. *Nat. Nanotechnol.* **2012**, 7, No. 803.

(35) Kurra, N.; Ahmed, B.; Gogotsi, Y.; Alshareef, H. N. MXene-on-Paper Coplanar Microsupercapacitors. *Adv. Energy Mater.* **2016**, 6, No. 1601372.

(36) Ko, Y.; Kwon, M.; Bae, W. K.; Lee, B.; Lee, S. W.; Cho, J. Flexible supercapacitor electrodes based on real metal-like cellulose papers. *Nat. Commun.* **2017**, 8, No. 536.

(37) Cao, R.; Pu, X.; Du, X.; Yang, W.; Wang, J.; Guo, H.; Zhao, S.; Yuan, Z.; Zhang, C.; Li, C.; Wang, Z. L. Screen-Printed Washable Electronic Textiles as Self-Powered Touch/Gesture Tribo-Sensors for Intelligent Human-Machine Interaction. *ACS Nano* **2018**, 12, 5190−5196.

(38) Choi, K.-H.; Yoo, J.; Lee, C. K.; Lee, S.-Y. All-inkjet-printed, solid-state flexible supercapacitors on paper. *Energy Environ. Sci.* **2016**, 9, 2812−2821.

(39) Hu, L.; Pasta, M.; Mantia, F. L.; Cui, L.; Jeong, S.; Deshazer, H. D.; Choi, J. W.; Han, S. M.; Cui, Y. Stretchable, porous, and conductive energy textiles. *Nano Lett.* **2010**, 10, 708−714.

(40) Cecen, V.; Seki, Y.; Sarikanat, M.; Tavman, I. H. FTIR and SEM analysis of polyester- and epoxy-based composites manufactured by VARTM process. *J. Appl. Polym. Sci.* **2008**, 108, 2163−2170.

(41) Huang, Y.; Ip, W. S.; Lau, Y. Y.; Sun, J.; Zeng, J.; Yeung, N. S. S.; Ng, W. S.; Li, H.; Pei, Z.; Xue, Q.; Wang, Y.; Yu, J.; Hu, H.; Zhi, C. Weavable, Conductive Yarn-Based NiCo//Zn Textile Battery with High Energy Density and Rate Capability. *ACS Nano* **2017**, 11, 8953−8961.

(42) Liang, H.; Meng, F.; Caban-Acevedo, M.; Li, L.; Forticaux, A.; Xiu, L.; Wang, Z.; Jin, S. Hydrothermal continuous flow synthesis and exfoliation of NiCo layered double hydroxide nanosheets for enhanced oxygen evolution catalysis. *Nano Lett.* **2015**, 15, 1421−1427.

(43) Nagaraju, G.; Chandra Sekhar, S.; Krishna Bharat, L.; Yu, J. S. Wearable Fabrics with Self-Branched Bimetallic Layered Double Hydroxide Coaxial Nanostructures for Hybrid Supercapacitors. *ACS Nano* **2017**, 11, 10860−10874.

(44) Li, B.; Quan, J.; Loh, A.; Chai, J.; Chen, Y.; Tan, C.; Ge, X.; Hor, T. S.; Liu, Z.; Zhang, H.; Zong, Y. A Robust Hybrid Zn-Battery with Ultralong Cycle Life. *Nano Lett.* **2017**, 17, 156−163.

(45) Yan, C.; Wang, X.; Cui, M.; Wang, J.; Kang, W.; Foo, C. Y.; Lee, P. S. Stretchable Silver-Zinc Batteries Based on Embedded Nanowire Elastic Conductors. *Adv. Energy Mater.* **2014**, 4, No. 1301396.

(46) Senguttuvan, P.; Han, S.-D.; Kim, S.; Lipson, A. L.; Tepavcevic, S.; Fister, T. T.; Bloom, I. D.; Burrell, A. K.; Johnson, C. S. A High Power Rechargeable Nonaqueous Multivalent Zn/V$_2$O$_5$ Battery. *Adv. Energy Mater.* **2016**, 6, No. 1600826.

(47) Wang, X.; Wang, F.; Wang, L.; Li, M.; Wang, Y.; Chen, B.; Zhu, Y.; Fu, L.; Zha, L.; Zhang, L.; Wu, Y.; Huang, W. An Aqueous Rechargeable Zn//Co$_3$O$_4$ Battery with High Energy Density and Good Cycling Behavior. *Adv. Mater.* **2016**, 28, 4904−4911.

(48) Kundu, D.; Adams, B. D.; Duffort, V.; Vajargah, S. H.; Nazar, L. F. A high-capacity and long-life aqueous rechargeable zinc battery using a metal oxide intercalation cathode. *Nat. Energy* **2016**, 1, No. 16119.

(49) Zhang, L.; Chen, L.; Zhou, X.; Liu, Z. Towards High-Voltage Aqueous Metal-Ion Batteries Beyond 1.5 V: The Zinc/Zinc Hexacyanoferrate System. *Adv. Energy Mater.* **2015**, 5, No. 1400930.

(50) Wang, F.; Borodin, O.; Gao, T.; Fan, X.; Sun, W.; Han, F.; Faraone, A.; Dura, J. A.; Xu, K.; Wang, C. Highly reversible zinc metal anode for aqueous batteries. *Nat. Mater.* **2018**, *17*, 543−549.

(51) Li, G.; Yang, Z.; Jiang, Y.; Jin, C.; Huang, W.; Ding, X.; Huang, Y. Towards polyvalent ion batteries: A zinc-ion battery based on NASICON structured Na3V2(PO4)3. *Nano Energy* **2016**, *25*, 211−217.

(52) Wan, F.; Zhang, L.; Dai, X.; Wang, X.; Niu, Z.; Chen, J. Aqueous rechargeable zinc/sodium vanadate batteries with enhanced performance from simultaneous insertion of dual carriers. *Nat. Commun.* **2018**, *9*, No. 1656.

(53) Yan, M.; He, P.; Chen, Y.; Wang, S.; Wei, Q.; Zhao, K.; Xu, X.; An, Q.; Shuang, Y.; Shao, Y.; Mueller, K. T.; Mai, L.; Liu, J.; Yang, J. Water-Lubricated Intercalation in V2O5·nH2O for High-Capacity and High-Rate Aqueous Rechargeable Zinc Batteries. *Adv. Mater.* **2018**, *30*, No. 1703725.

(54) Li, H.; Liu, Z.; Liang, G.; Huang, Y.; Huang, Y.; Zhu, M.; Pei, Z.; Xue, Q.; Tang, Z.; Wang, Y.; Li, B.; Zhi, C. Waterproof and Tailorable Elastic Rechargeable Yarn Zinc Ion Batteries by a Cross-Linked Polyacrylamide Electrolyte. *ACS Nano* **2018**, *12*, 3140−3148.

(55) Zou, P.; Wang, Y.; Chiang, S.-W.; Wang, X.; Kang, F.; Yang, C. Directing lateral growth of lithium dendrites in micro-compartmented anode arrays for safe lithium metal batteries. *Nat. Commun.* **2018**, *9*, No. 464.

(56) Liu, Y.; Lin, D.; Jin, Y.; Liu, K.; Tao, X.; Zhang, Q.; Zhang, X.; Cui, Y. Transforming from planar to three-dimensional lithium with flowable interphase for solid lithium metal batteries. *Sci. Adv.* **2017**, *3*, No. eaao0713.

(57) Hu, H.; Yang, X.; Zhai, F.; Hu, D.; Liu, R.; Liu, K.; Sun, Z.; Dai, Q. Far-field nanoscale infrared spectroscopy of vibrational fingerprints of molecules with graphene plasmons. *Nat. Commun.* **2016**, *7*, No. 12334.

(58) Pu, X.; Li, L.; Liu, M.; Jiang, C.; Du, C.; Zhao, Z.; Hu, W.; Wang, Z. L. Wearable Self-Charging Power Textile Based on Flexible Yarn Supercapacitors and Fabric Nanogenerators. *Adv. Mater.* **2016**, *28*, 98−105.

(59) Lin, Y.-C.; Li, M.; Wu, C.-C. Simulation and experimental demonstration of the electric field assisted electroporation microchip for in vitro gene delivery enhancement. *Lab Chip* **2004**, *4*, 104−108.